THE JOURNAL OF BIOLOGICAL CHEMISTRY VOL. 284, NO. 31, pp. 20699–20707, July 31, 2009

The Biological Activity of the Prototypic Cyclotide Kalata B1 Is Modulated by the Formation of Multimeric Pores*[S]

Received for publication, April 4, 2009, and in revised form, May 21, 2009 Published, JBC Papers in Press, June 1, 2009, DOI 10.1074/jbc.M109.003384

Yen-Hua Huang[‡1], **Michelle L. Colgrave**[‡§], **Norelle L. Daly**[‡], **Asbed Keleshian**[¶], **Boris Martinac**[¶2], **and David J. Craik**[‡2,3]

From the [‡]*Institute for Molecular Bioscience and* [¶]*School of Biomedical Science, The University of Queensland, and* [§]*CSIRO Division of Livestock Industries, CSIRO, Brisbane 4072, Australia*

The cyclotides are a large family of circular mini-proteins containing a cystine knot motif. They are expressed in plants as defense-related proteins, with insecticidal activity. Here we investigate their role in membrane interaction and disruption. Kalata B1, a prototypic cyclotide, was found to induce leakage of the self-quenching fluorophore, carboxyfluorescein, from phospholipid vesicles. Alanine-scanning mutagenesis of kalata B1 showed that residues essential for lytic activity are clustered, forming a bioactive face. Kalata B1 was sequestered at the membrane surface and showed slow dissociation from vesicles. Electrophysiological experiments showed that conductive pores were induced in liposome patches on incubation with kalata B1. The conductance calculated from the current-voltage relationship indicated that the diameter of the pores formed in the bilayer patches is 41–47 Å. Collectively, the findings provide a mechanistic explanation for the diversity of biological functions ascribed to this fascinating family of ultrastable macrocyclic peptides.

The cyclotides are a family of topologically unique macrocyclic peptides abundant in plants of the Rubiaceae (coffee) and Violaceae (violet) families. They possess unusual structural and biophysical properties and are composed of a head-to-tail cyclic backbone and a cystine knot (1). The cystine knot is formed by a disulfide bond that penetrates a ring made by two other disulfide bonds and their connecting backbone segments. The structure of kalata B1, the prototypic cyclotide, is illustrated in Fig. 1 (2). The cyclic cystine knot at the core of three-dimensional structure contributes to the exceptional chemical and biological stability of cyclotides (3) and underpins their exciting potential for pharmaceutical and agricultural applications (4).

Cyclotides display a diverse range of biological activities, including anti-human immunodeficiency virus (5–8), neurotensin antagonism (9), hemolytic (10), antimicrobial (11), antifouling (12), and pesticidal activities (13–19). Cyclotides have been postulated to be defense-related proteins on the basis of their pesticidal activity and the suite of natural isoforms present in individual plants (20). Little is known about their mechanism of action, but their observed activities potentially might be associated with membrane interactions. Studies utilizing analytical ultracentrifugation (21) have shown that the cyclotide kalata B2 forms specific oligomers in solution, which could potentially have a role in the formation of membrane-spanning pores. A membrane-based mechanism of action is supported by a recent surface plasmon resonance study, which demonstrated that several kalata-like cyclotides bind to phosphatidylethanolamine-containing membranes (22). More recently, the cyclotide cycloviolacin O2 was shown to be cytotoxic to a human lymphoma cell line and induce leakage of calcein-loaded HeLa cells (23). NMR studies showed that the binding of kalata B1, and other analogues, to dodecylphosphocholine micelles is modulated by both electrostatic and hydrophobic interactions (24, 25). Although these findings indicate that cyclotides interact with a wide range of membranes, with incorporation of the cyclotide structure into monolayers (micelles), and result in leakage of cellular contents from bilayers (HeLa cells), a functional study of cyclotide-membrane interactions is to date lacking.

In the present study, the membrane-binding ability of prototypic cyclotide kalata B1 is delineated, and the mechanism of action is defined. For the first time we show that cyclotides form pores with channel-like activities in membranes. Dye leakage experiments indicate that kalata B1 induces membrane permeability, and electrophysiological measurements provide unequivocal evidence of pore formation, probably involving the insertion of oligomers of kalata B1 into the lipid bilayers. The results indicate that the diverse range of biological activities reported for cyclotides can be accounted for by membrane permeabilization associated with transmembrane pores with channel-like activity.

EXPERIMENTAL PROCEDURES

Protein Purification—Native kalata B1 was isolated from the above ground parts of *Oldenlandia affinis* and purified as described previously (4). The concentration of the peptide was determined spectrophotometrically using an extinction coefficient of 5875 M^{-1} cm^{-1} at 280 nm.

Synthesis of Alanine Mutants—Alanine mutants of kalata B1 were synthesized using solid-phase methods as previously described (26). Briefly, the peptides were assembled using manual solid-phase peptide synthesis with *t*-butoxycarbonyl chemistry. Amino acids were added to the resin using 2-(1-*H*-benzotriazol-1-yl)-1,1,3,3-tetramethyluronium hexafluoro-

* This work was supported in part by grants from the Australian Research Council (to D. J. C. and B. M.) and by an Australian Research Council-Commonwealth Scientific and Industrial Research Organization (CSIRO) Linkage Grant (to M. L. C.).

[S] The on-line version of this article (available at http://www.jbc.org) contains supplemental Fig. S1.

[1] Supported by an Institute for Molecular Bioscience-CSIRO Ph.D. Scholarship.
[2] ARC Professorial Fellows.

[3] To whom correspondence should be addressed: Institute for Molecular Bioscience, The University of Queensland, Brisbane 4072, Australia. Tel.: 617-33-462-019; Fax: 617-33-462-029; E-mail: d.craik@uq.edu.au.

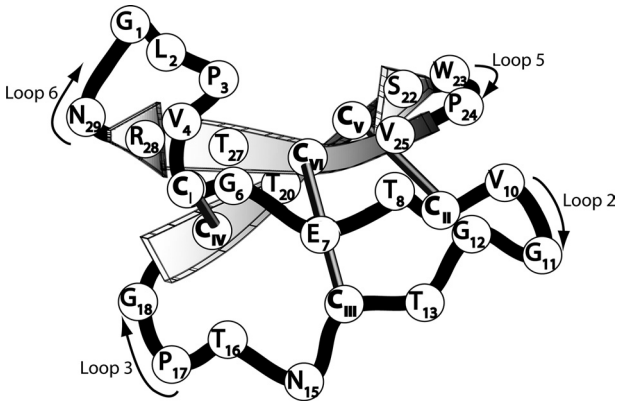

FIGURE 1. **Structural representation of the kalata B1 sequence showing the cystine knot topology and head-to-tail cyclized backbone (PDB ID 1nb1).** The six cysteine residues are *bolded* and labeled with *Roman numerals*. The three disulfide bonds are shown as *cylinders* connecting the cysteine residues (*I–IV*, *II–V*, and *III–VI*). The backbone segments between successive cysteine residues are referred to as loops. *Loops 2*, *3*, *5*, and *6* are marked, with the *small arrows* indicating the direction of the peptide chain from amino to carboxyl ends. *Loops 1* and *4* form part of the embedded ring of cystine knot. The *broad arrows* indicate β-strands in the peptide backbone that are typically associated with cystine knot motifs (47).

phosphate with *in situ* neutralization. Cleavage of the peptides from the resin was achieved using hydrogen fluoride with *p*-cresol and *p*-thiocresol as scavengers (9:0.8:0.2 v/v, HF:cresol:thiocresol). The crude reduced peptides were purified on a Phenomenex C_{18} column. Gradients of 0.05% aqueous trifluoroacetic acid and 90% acetonitrile, 0.045% trifluoroacetic acid were employed with a flow rate of 8 ml/min, and the eluant was monitored at 230 nm. These conditions were used in subsequent purification steps. Cyclization and oxidation of the mutants were performed by dissolving the peptides in 50/50 (v/v) 0.1 M ammonium bicarbonate (pH 8)/isopropanol (0.5 mg/ml). The mixture was stirred at room temperature overnight and then purified by reversed phase-high performance liquid chromatography. Correctly folded mutants were identified by their late elution under reversed phase conditions, and ^{1}H NMR spectra confirmed the folded states. All peptides were characterized using electrospray ionization mass spectrometry, and the purity was checked with analytical high performance liquid chromatography.

As reported earlier (18), the Trp-23 and Pro-24 mutants did not fold under the folding conditions used for the other mutants. Additional folding trials confirmed that the Trp-23 mutant could be folded with the addition of 1 mM glutathione to the folding buffer. The folding of W23A was confirmed using NMR spectra: the αH shifts of W23A mirrored those of the native peptide (supplemental Fig. S1*A*). The P24A mutant was insoluble, presumably because of incorrect folding, and was not further examined.

Hemolytic Assay—A hemolytic assay was conducted on mutant W23A using a method similar to that described previously (18) for the other mutants. Data for the other Ala mutants were available from the previous study. Human erythrocytes were separated from serum with repeated centrifugation at 4000 rpm in phosphate-buffered saline (pH 7.4). A pellet of erythrocytes was resuspended to a 0.25% (v/v) solution. Stock solutions of the peptide were prepared at 300 μM then serially diluted in triplicates and were aliquoted into a 96-well plate. 100 μl of the 0.25% erythrocyte solution was dispensed into each well and incubated with diluted peptide solution at 37 °C for 1 h. The 96-well plate was centrifuged to pellet the intact red blood cells, and the supernatant of each well was measured by visual absorption spectroscopy at 415 nm.

Vesicle Preparation—Vesicles were prepared as described previously (27). The standard buffer was composed of 10 mM HEPES (from Sigma-Aldrich), 107 mM NaCl, 1 mM $Na_2EDTA{\cdot}2H_2O$, and ~5–6 mM NaOH to adjust the pH to 7.4.

The fluorescent dye 5-carboxyfluorescein (CF)[4] was purchased from Sigma-Aldrich. An aqueous stock was prepared containing 50 mM CF in standard buffer and was adjusted using NaOH to pH7.4. The dye solution was stored at 4 °C in the dark.

The lipids 1-palmitoyl-2-oleoyl-*sn*-glycero-3-phosphatidylcholine (POPC), 1-palmitoyl-2-oleoyl-*sn*-glycero-3-(phospho-*rac*-(1-glycerol)) (POPG), 1-palmitoyl-2-oleoyl-*sn*-glycero-3-phosphoethanolamine (POPE), cholesterol, and sphingomyelin (SM) were purchased from Avanti Polar Lipids. 20 mg of each lipid was dissolved in 2 ml of chloroform (Sigma-Aldrich) separately and then dried under a stream of nitrogen gas and then vacuum-desiccated overnight. Lipids were stored under nitrogen at −20 °C to prevent oxidation. Lipid concentrations were determined by the Stewart assay (28).

Dry lipid was dispersed in the standard buffer (in the absence or presence of dye) by vortex mixing, followed by sonication at 25 °C under nitrogen for 45 min. The liposome solutions were then sized 19 times by extrusion through two stacked 100 nm Nucleopore polycarbonate membranes (Avanti Polar Lipids). Vesicles loaded with CF were separated from non-entrapped dye on a Sephadex G-50 column (Amersham Biosciences). Several membrane systems were prepared, including vesicles composed of a single phospholipid (POPC or POPG), as well as vesicles with a mixed phospholipid composition POPC/POPE/SM/cholesterol (2:2:3:1) to imitate the outer membranes of human erythrocyte (29). Two other analogue lipid systems lacking either cholesterol (POPC/POPE/SM) or sphingomyelin (POPC/POPE/cholesterol) were also examined against kalata B1. The vesicles were diluted to a lipid concentration of 100 μM with standard buffer before addition of peptide.

Leakage of Vesicle Contents—Preliminary fluorescence emission spectra were measured between 460 and 600 nm on a PerkinElmer Life Sciences luminescence spectrometer with a scan speed of 140 nm/min. An excitation wavelength of 480 nm and a quartz cuvette with an optical path width of 4 mm were used. The excitation and emission slit widths were set to 4 nm. Experiments were performed at 25 °C. The initial fluorescence signal, F_o (when cells/vesicles are intact, *i.e.* no leakage), was measured, and each run was started by the addition of 50 μl of a peptide solution. Fluorescence spectra were measured every minute for 20 min before the addition of 1% (v/v) Triton X-100 solution, whereby the vesicles are completely lysed giving rise to the formation of mixed micelles and yielding a fluorescence

[4] The abbreviations used are: CF, carboxyfluorescein; POPC, 1-palmitoyl-2-oleoyl-*sn*-glycero-3-phosphatidylcholine; POPG, 1-palmitoyl-2-oleoyl-*sn*-glycero-3-[phospho-*rac*-(1-glycerol)]; POPE, 1-palmitoyl-2-oleoyl-*sn*-glycero-3-phosphatidylethanolamine; SM, sphingomyelin.

signal of maximum intensity, F_x. Control experiments were conducted with the addition of Milli Q H_2O only. A miniaturized version of the assay was set up using a 96-well plate format. Vesicles were prepared as described above and were aliquoted into the wells. The test peptides were added to each well, thoroughly mixed by pipette aspiration, and incubated at room temperature for a minimum of 20 min prior to fluorescence measurements. The fluorescence intensity of the released CF solutions was read using an Envision 2102 Multilabel Reader with excitation at 485 nm and emission at 528 nm. All experiments were conducted in triplicate, and controls with H_2O alone (spontaneous dye release) were used. Following measurement of dye release from vesicles incubated with cyclotide, Triton X-100 was added, and the fluorescence was measured to obtain F_x.

Starting with a self-quenching concentration of CF (50 mM) inside the vesicles, leakage of the dye resulting from incubation of the vesicles with cyclotides was detected as an increase in fluorescence intensity, due to dilution below self-quenching concentrations. The spontaneous leakage of CF in the absence of peptide was found to be negligible. From the observed fluorescence during the measurement period, a normalized efflux function (30, 31) that describes the efflux over the period of the experiment was determined according to:

$$E(t) = \frac{F_x - F(t)}{F_x - F_0} \qquad \text{(Eq. 1)}$$

where $F(t)$ is the measured fluorescence at time t, F_o is the initial fluorescence before addition of peptide, and F_x is the final fluorescence after addition of 1% (v/v) Triton X-100. The leakage of a dye (which varies between 0 and 100%) was calculated according to the equation (27), % Leakage $= (1 - E(t)) \times 100$. Leakage of aqueous vesicle contents to the external medium was monitored using the CF assay, by the addition of varying amounts of the cyclotide kalata B1 from a stock solution to unilamellar vesicle suspensions.

Irreversible Binding Experiments—POPC/POPE/cholesterol (5:3:2) vesicles were prepared in standard buffer (no dye) or in standard buffer containing dye. A series of kalata B1 solutions was prepared via serial dilution, and these were preincubated with the dye-free vesicles (no CF) for 30 min at 25 °C. The mixture was then incubated with CF-entrapped vesicles to give a 50:50 mixture of dye-free:dye-containing vesicles prior to measuring the fluorescence intensity. In parallel, solutions of the same peptide concentrations were incubated with a 50:50 mixture of dye-free and dye-containing vesicles, *i.e.* no preincubation period, before measuring their fluorescence intensity.

Preparation of Liposomes—Liposomes were formed from asolectin (soybean lecithin, Sigma) based on a procedure described previously (32, 33). The asolectin contained several carbon chains, 60% of which were comprised by 18:2. Briefly, 2 mg of the asolectin was dissolved in chloroform (Sigma-Aldrich), evaporated, and dried under a nitrogen jet for 15 min. To achieve a 10 mg/ml solution in final concentration, the thin layer of lipid was then dispersed in 200 μl of dehydration/rehydration buffer (D/R buffer, 200 mM KCl/5 mM HEPES/KOH, pH 7.2) by vortex mixing, followed by sonication for 5–15 min at room temperature to obtain a cloudy liquid. The liquid was transferred to a 15-ml centrifuge tube (diluted to 3 ml) and placed on a platform rocker for 3 h at room temperature. The solution was spun for 30 min at 90,000 rpm at 4 °C (TL-100 Ultracentrifuge, Beckman) to obtain a pellet of liposome. The pellet (2 mg of asolectin) was resuspended in 40 μl of D/R buffer and two of 10-μl (0.5 mg) aliquots were spotted onto an ethanol-cleaned slide. The spots were then dehydrated and desiccated under vacuum overnight and rehydrated on the next day for at least 6 h.

Electrophysiological Measurements—Excised liposome patches were used for these experiments. The liposome spot was rehydrated with 10 μl of D/R buffer on the day before the operation of patch clamping. For patch clamping, 10 μl of D/R buffer was used to disperse a quarter of the liposome spot that had been rehydrated overnight and transferred to a chamber containing 700 μl of recording solution (D/R buffer with additional 40 mM $MgCl_2$, pH 7.2). Clear blisters were observed to form within 15 min of plating under an optical phase-contrast microscope for imaging low contrast, transparent samples such as blisters of monolayer. Channel currents were recorded by using borosilicate micropipettes with a bubble number of 3.2 to 2.6, which corresponds to a resistance of 4–6 MΩ with recording solution in the pipette and bath. A seal was formed on the pipette tip directly after the pipette contacted the surface of the blister or alternatively after a light suction was applied. To prevent the free ends of the patch resealing, the pipette was lifted to pass through the air interface quickly. The patch current signal was amplified, filtered (1 kHz), and digitized at 5 kHz with a computer using software PCLAMP9. Different concentrations of either the kalata B1, the inactive V25A-kB1 mutant, or the active T20A-kB1 mutants were placed in the pipette solution in separate experiments. The potassium present in the normal recording solution was substituted separately with an equimolar concentration of sodium or the large cation, *N*-methyl-D-glucamine, to assess the cation-selective properties of the channel-like pores that kalata B1 induced in asolectin liposomes.

RESULTS

Kalata B1 Induces Leakage in Model Membrane Mimetics—Phospholipid vesicles have been used extensively to investigate the properties of biological membranes and their interactions with ligands. Fluorescence spectroscopy is a sensitive technique that detects binding ability and membrane perturbation by measuring the release of fluorescent dyes from vesicles. In the current study, vesicles were loaded with a self-quenching fluorescent dye, CF, as a probe to monitor vesicle leakage. At high concentrations, *i.e.* within the vesicle, the fluorescence intensity is weak due to self-quenching; however, upon pore formation or other disruption of the lipid bilayer, the dilution of the fluorophore results in an increase in fluorescence intensity, which can be measured over time. This approach was used to investigate cyclotide-induced leakage of a self-quenching dye from a variety of lipid systems. The first leakage experiment used zwitterionic vesicles composed of 100% POPC (16:0–18:1). The phosphatidylcholine headgroup is a major component of biological membranes. To evaluate potential electrostatic

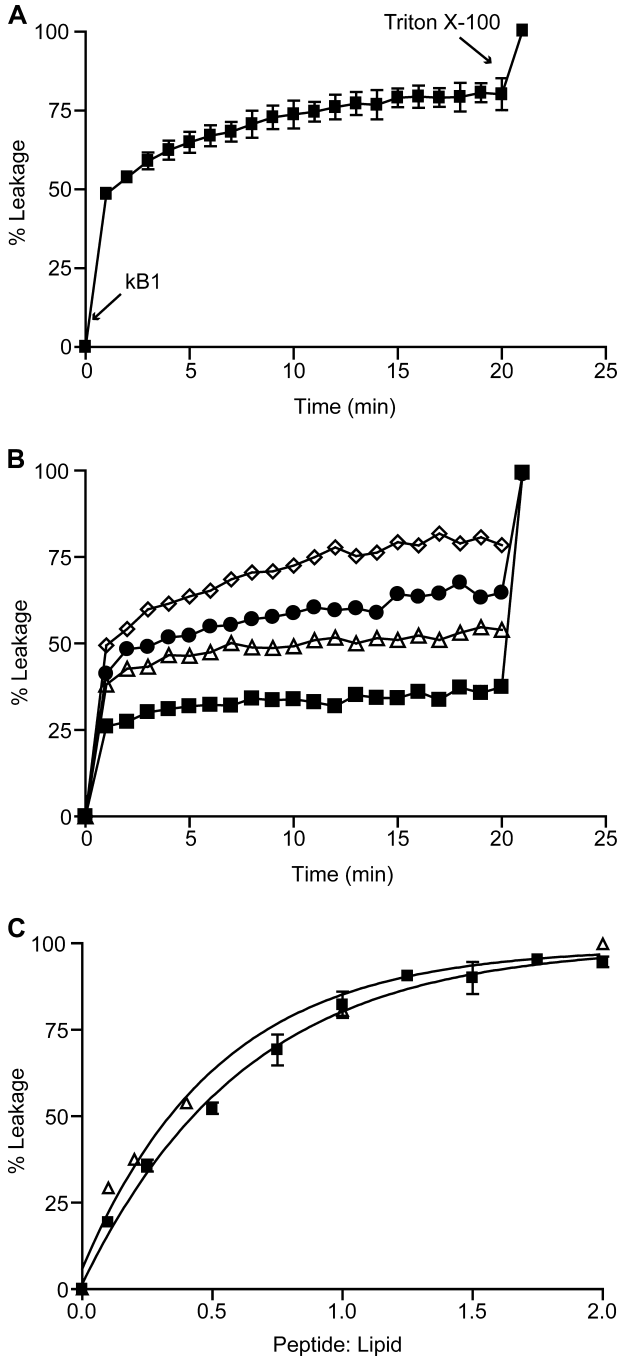

FIGURE 2. **Kalata B1-induced leakage of CF from unilamellar vesicles.** *A*, time course of the fluorescence signal during efflux measurement from 0 to 20 min following addition of 100 μM kalata B1 to POPC vesicles. The *first arrow* indicates the addition of peptide to 100 μM POPC liposome solution, and the *squares* represent readings recorded at 1-min intervals. The *second arrow* corresponds to the addition of 1% Triton X-100, which results in complete lysis of the membrane and 100% leakage of the vesicle contents. *B*, the release of CF from 100 μM POPC vesicles as a function of time for four different kalata B1 concentrations (*solid squares*, 25 μM; *open triangles*, 50 μM; *solid circles*, 75 μM; *open diamonds*, 100 μM). *C*, curves of kalata B1-induced leakage of CF from POPC (*solid squares*) and POPG (*open triangles*) vesicles. The fluorescence intensities from individual experiments after 20 min were converted to percentage leakage values and plotted as a function of the peptide:lipid ratio.

interactions of kalata B1, the anionic phospholipid POPG was used in other experiments.

Fig. 2*A* shows the time course for a typical efflux measurement from a POPC vesicle solution for which the background

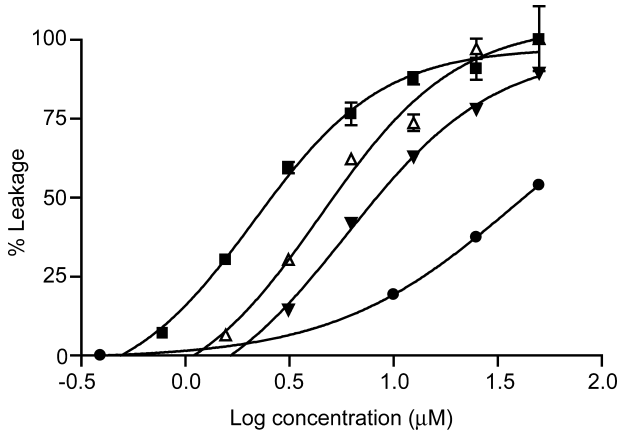

FIGURE 3. **Kalata B1-induced leakage of CF from vesicles of mixed lipid composition.** Vesicles composed of POPC/POPE/SM/cholesterol (2:2:3:1, *solid squares*) were used to represent mammalian cell membranes, whereas vesicles composed of POPC (*solid circles*) were used to represent single lipid system with fluid phase. Two other analogue lipid systems lacking either cholesterol (POPC/POPE/SM, *open triangles*) or sphingomyelin (POPC/POPE/cholesterol, *solid reversed triangles*) were also tested.

fluorescence was measured before the addition of kalata B1 at $t = 0$ min. Subsequent measurements were taken at 1-min intervals for 20 min, after which 1% (v/v) Triton X-100 was added. Triton addition corresponded with complete lysis of the membrane, and thus 100% leakage of the vesicle contents. The fluorescence maximum occurred at 518 nm. The fluorescence data were converted to efflux values, $E(t)$, and subsequently to percentage leakage values. Fig. 2*B* shows a time course of the fluorescence signal during an efflux measurement from POPC vesicles for four cyclotide concentrations. Leakage occurred rapidly, with >50% of the total fluorescence intensity observed after 1 min, followed by a gradual increase in fluorescence for up to 10 min. At any given cyclotide concentration, leakage was effectively complete after 10 min, and so the CF fluorescence intensity 20 min after peptide addition was used as a measure of the total peptide-induced dye leakage. Similar traces were obtained at both lower and higher POPC vesicle concentrations (data not shown). These experiments showed that cyclotides are capable of altering membrane permeability, leading to loss of the internal vesicle contents to the external medium. Kalata B1 showed a similar concentration-dependent effect on POPC and POPG vesicles (Fig. 2*C*) and caused 100% leakage at peptide-to-lipid ratio of 2:1 for both model membranes.

Fig. 3 shows the kalata B1-induced leakage of CF from vesicles of mixed lipid composition. POPC/POPE/SM/cholesterol (molar ratio, 2:2:3:1) was selected to represent mammalian cell membranes, such as human erythrocytes (29), and was compared with a single lipid system composed of pure POPC or mixed lipid systems lacking either cholesterol or sphingomyelin. Compared with POPC alone (EC_{50} = 37.8 μM), kalata B1 showed a greater affinity for vesicles consisting of POPC/POPE/SM/cholesterol (EC_{50} = 2.1 μM). The concentration-response curves of two other vesicles lacking sphingomyelin (5.9 μM) or cholesterol (4.5 μM), showed kalata B1 had decreased affinity for these lipid compositions.

Alanine Mutation Reveals an Active Face—A suite of 22 single point alanine mutants of kalata B1 was synthesized and examined in dye leakage experiments to determine the residues

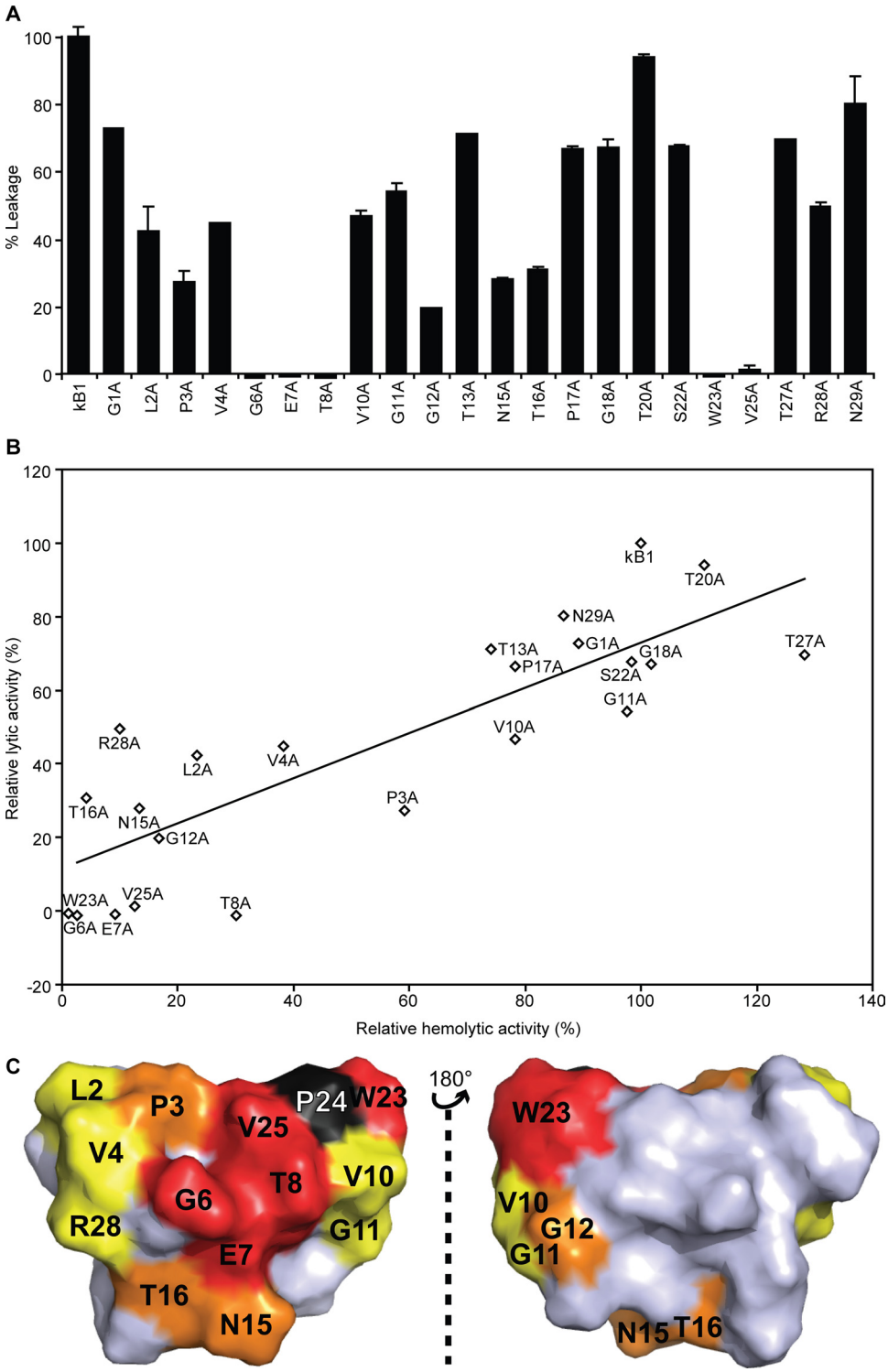

FIGURE 4. **Comparison of the percentage leakage of CF from POPC/POPE/cholesterol (5:3:2) vesicles induced by alanine mutants of kalata B1 using 50 μM cyclotide or analogue concentration.** *A*, percentage leakage caused by alanine mutants standardized using wild-type kalata B1 as 100%. *B*, correlation between lytic and hemolytic activity of alanine mutants. *C*, surface representation showing the residues critical to lytic activity of kalata B1. Alanine mutation of residues shown in *red* reduced lytic ability of kalata B1 to <5%, when those in orange decreased to 20–40% and in *yellow* to 40–60%. The P24 mutant (*black*) was insoluble in the folding buffer and hence could not be tested.

responsible for the lytic ability of the peptide. The mutants were tested at 50 μM and compared with wild-type kalata B1, which resulted in 100% leakage at this concentration. Fig. 4*A* shows the results of triplicate measurements for each of the alanine mutants. Substitution of any residue in loop 1 (see Fig. 1 for loop definitions) of kalata B1, by Ala, was observed to abolish the lytic ability of the peptide, as did mutation of Trp-23 or Val-25 in loop 5. The lack of activity of these mutants was not due to incorrect folding, because their αH shifts corresponded closely to those of the native peptide reported previously (18), consistent with them having the same global fold.

The G12A mutation in loop 2, the N15A and T16A mutations in loop 3, and the P3A mutation in loop 6 resulted in significant (~75%), but not complete, loss of activity. These results correlate well with trends in the hemolytic activity against human erythrocytes (18) of a series of alanine mutants of kalata B1, as shown in Fig. 4*B*. Fig. 4*C* shows a three-dimensional representation of the residues critical to the lytic ability of kalata B1 (Gly-6, Glu-7, Thr-8, Trp-23, and Val-25). Mutations that caused a significant decrease, *i.e.* 20–40% of the activity of wild-type kalata B1 (Gly-12, Asn-15, Thr-16, and Pro-3) or a slight decrease, *i.e.* reduced lytic activity to 40–60% (Val-10, Gly-11, Arg-28, Leu-2, and Val-4) are also depicted. Notably, residues responsible for lytic ability are localized on one surface of kalata B1.

Kalata B1 Is Sequestered on the Membrane Surface—The reversibility of the interaction of kalata B1 with phospholipid membranes was investigated using a 50:50 mixture of dye-loaded and dye-free vesicles (34). We found that at 12.5 or 25 μM concentrations the percentage leakage for a 50:50 mixture of dye-loaded and dye-free vesicles was equivalent to 100% dye-loaded vesicles (data not shown). Therefore the peptide did not discriminate between the dye-loaded or dye-free vesicles, *i.e.* the membrane properties did not change in the presence or absence of the fluorescent dye. To explore the kinetics of association of kalata B1 with the phospholipid vesicles, the leakage of CF was monitored over 90 min (Fig. 5). The majority of lysis (80%) occurred over the first 2.5 min for the 50:50 mixture of dye-loaded and dye-free vesi-

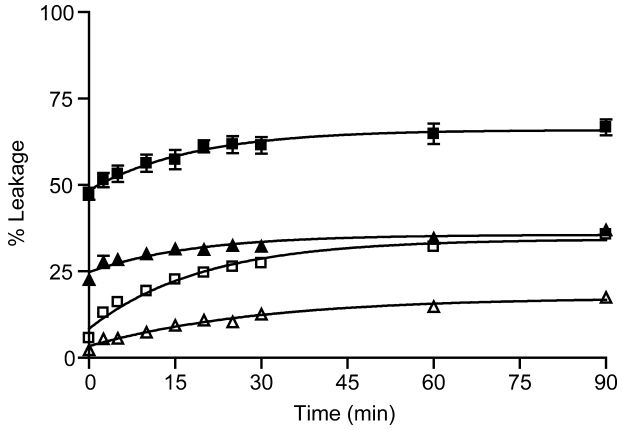

FIGURE 5. **Reversibility of the kalata B1-membrane interaction.** Time course for kalata B1-induced leakage of CF from a 50:50 mixture of dye-loaded:dye-free POPC/POPE/cholesterol (5:3:2) vesicles. Peptide concentrations of 25 μM (*squares*) and 12.5 μM (*triangles*) were used. The peptide was added immediately (*solid symbol*) to a 50:50 mixture of vesicles or preincubated for 30 min (*open symbol*) with dye-free vesicles prior to incubation with dye-loaded vesicles.

cles, with a calculated half-life of ~0.5 min. This was also the case for the leakage of CF from solutions containing 100% dye-loaded vesicles. In a separate experiment, kalata B1 was preincubated with dye-free vesicles for 30 min, prior to the addition of dye-loaded vesicles. In this system, lysis occurred at a slower rate, with 80% of leakage occurring after 30 min, and reached a maximum of approximately half of the value obtained for the lysis from the mixed vesicles without a preincubation period. The calculated half-life for leakage from the dye-containing vesicles following the preincubation was >5 min (representing a 10-fold increase over the case with no preincubation). This trend took place at both concentrations of kalata B1 and indicates that slow exchange of peptide molecules between the vesicles occurs, with ~25% of the peptide available to cause lysis of the dye-loaded vesicles following the preincubation.

Kalata B1 Forms Conductive Pores—Patch clamp recording was developed to understand the electrophysiology of cellular membranes by measuring ion currents passing through the membranes of biological cells (35–39). In the current study, the patch clamp technique was used to examine cyclotide-induced ion conduction through lipid bilayers. Asolectin is commonly used in membrane studies for the reconstitution of phospholipid vesicles. Asolectin contains a mixture of phospholipids, with the three main headgroups being choline, ethanolamine, and inositol (33).

Fig. 6*A* shows a typical current recording from a liposome patch to which a 25 μM kalata B1 solution was applied. No channel activity was observed during the first 190 s, after which a progressive staircase of currents with amplitudes of ~120 pA occurred, lasting for ~28 s, until the liposome patch ruptured. The *inset* in Fig. 6*A* shows discrete current fluctuations, between 110 and 130 pA, on an enlarged time scale. Overall, the data suggest that the mode of action of kalata B1 involves the formation of membrane pores with channel-like activity. Similar effects were observed at concentrations down to 2.5 μM, with the time of onset of conductance increasing with a decrease in peptide concentration (onset time between 10 and 15 min). For example, the *current trace* shown in Fig. 6*B* is

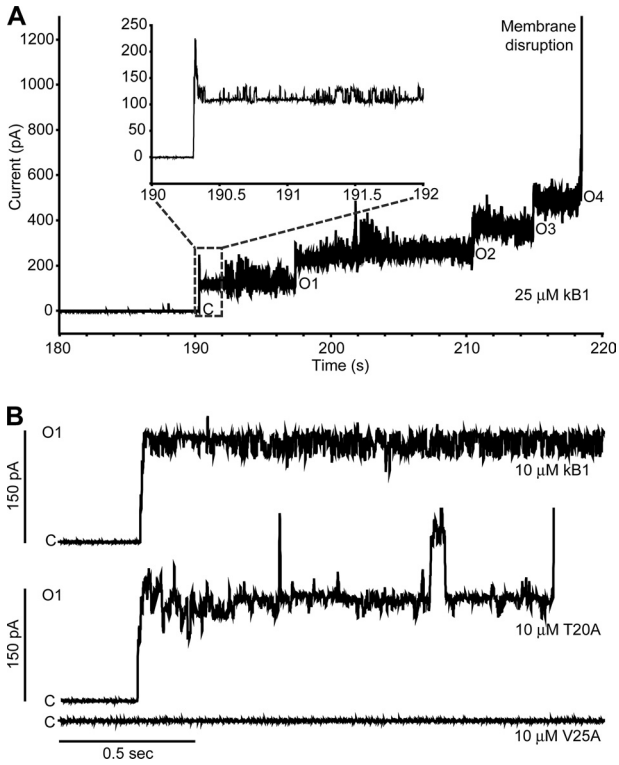

FIGURE 6. **Recordings of patches isolated from asolectin liposomes when different concentrations of kalata B1 solution are present in the pipettes.** The patch potentials are +30 mV in each case. *A*, recording of current steps when 25 μM kalata B1 solution was present in the pipette solution. The *upper panel* shows the enlargement of the region highlighted in the *lower panel*. *B*, shows typical current traces when 10 μM kalata B1, 10 μM T20A-kB1, and 10 μM V25A-kB1 were applied, respectively. The alanine mutant V25A-kB1, which was inactive in the membrane leakage experiments, was selected as a negative control and showed no activity in the patch clamp experiments.

characteristic of recordings for 10 μM kalata B1. Patch clamp experiments with a kalata B1 concentration of 100 μM were also attempted, but no current could be recorded, because the patch broke upon gigaohm seal formation. This observation suggests that the insertion of the peptide into the membrane occurred very rapidly when high concentrations of kalata B1 were applied.

No channel-like activity was recorded in any of the 50+ experiments for patches without kalata B1 in the pipette recording solution. Additionally, positive and negative control alanine mutants were tested in the patch clamp experiments; these included an active T20A-kB1 mutant and an inactive V25A-kB1 mutant from the membrane leakage experiments. The T20A mutant gave similar results to the wild type at a concentration of 10 μM, as shown in Fig. 6*B*. V25A-kB1 did not exhibit channel-like activity compared with the control, as shown in the *bottom panel* in Fig. 6*B*.

Having established that the increase in membrane conductance induced by kalata B1 in liposome patches can be attributed to the opening of pores formed by the peptide, we changed the ions in the recording solution to test the specificity of the pores. Substitution of potassium ions for sodium ions or a large cation, *N*-methyl-D-glucamine, did not reduce the ionic current, which suggests that the pores are not selective for specific cations.

Experiments were then undertaken to determine the size of the pores. Fig. 7 shows a plot of the current-voltage (I/V) rela-

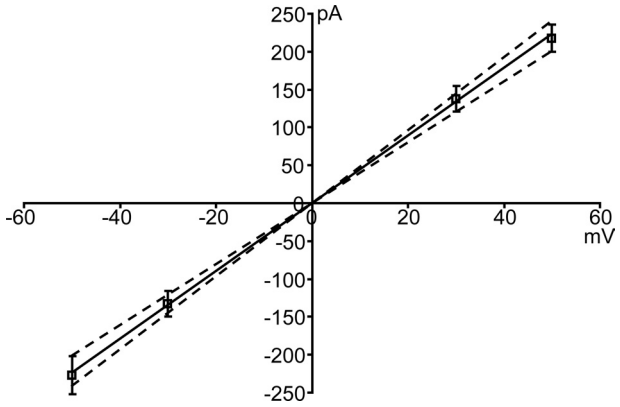

FIGURE 7. **The I/V plot of kalata B1 induced ion current changes on asolectin liposome patch.** The current-voltage relationship when 2.5 μM kalata B1 is present in the normal recording solution is shown. Currents were measured at pipette voltages between −50 mV and +50 mV, and each data point represents the average obtained from more than three individual measurements. Linear regression analysis gave an average conductance value of 4.46 nS (*solid line*) with lower and upper limits of 4.01 and 4.82 nS (*dashed lines*).

tionship recorded from asolectin liposome patches to which 2.5 μM kalata B1 was applied. Ion current fluctuations were detected in the presence of kalata B1 solution. A primary channel-like opening event (first step) was observed for 37 of 86 readings, with amplitudes of 120–150 pA recorded upon application of +30 mV pipette voltage. The amplitude of the current was plotted against the pipette potential (varied from −50 mV to +50 mV) as shown in Fig. 7. A linear relationship was observed, and the slope of the I/V plot indicated an average conductance of 4.46 nS. Equation modified by Cruickshank *et al.* (40) was used to estimate the diameter of the pores formed by kalata B1,

$$d = \frac{pg}{\pi}\left(\frac{\pi}{2} + \sqrt{\frac{\pi^2}{4} + \frac{4\pi l}{pg}}\right) \qquad \text{(Eq. 2)}$$

where d is diameter, ρ is resistivity of recording solution, g is conductance, and l is minimum length of the membrane-spanning region. The diameter of the pores was calculated to be 44.4 Å (range: 41.4–46.8 Å) based on the measured conductance values, the resistivity of the recording solution ($\rho = 49.7\ \Omega$ cm), and the length of the membrane spanning region (l = 35 Å).

DISCUSSION

In this study the mode of action of cyclotides was explored using the prototypic cyclotide kalata B1, a suite of alanine mutants, a range of model membrane systems, and multidisciplinary biophysical and electrophysiological approaches. The data unequivocally show that cyclotides interact with membranes, form pores with channel-like activity, and functionally facilitate the leakage of vesicular contents.

Two simple model membrane systems were examined, one containing the zwitterionic phospholipid POPC and the other the anionic phospholipid POPG. In broad terms, the leakage of dye induced by kalata B1 from the two membrane mimetics was similar. Kalata B1 showed an increased lytic ability upon incorporation of POPE in the vesicle systems. Likewise, kalata B1 had an increased lytic effect on multicomponent membranes incorporating POPE, cholesterol, and sphingomyelin, which better represent a true biological membrane. Slight decreases in affinity were observed in vesicles lacking either sphingomyelin or cholesterol, with the effect being more pronounced for vesicles lacking sphingomyelin.

Alanine scanning mutagenesis revealed a series of residues that, upon substitution, resulted in mutants that caused significantly less leakage across membranes than the wild-type kalata B1. These residues clustered to form a bioactive face, illustrated in Fig. 4*C*. All three residues in loop 1 (Gly-6, Glu-7, and Thr-8), and Trp-23 and Val-25 in loop 5, are critical for the membranelytic activity of kalata B1. The Gly-12 residue in loop 2, Asn-15 and Thr-16 in loop 3, and Pro-3 in loop 6 affect activity to a lesser degree. According to a study by Simonsen *et al.* (18), substitution of the highly conserved glutamic acid (Glu-7) in loop 1 of the cyclotide family with alanine leads to a loss of a network of hydrogen bonds involving Glu-7 and hence the loss of structural stability. The G12A mutant is the only "bioactive" residue not clustered with the other critical residues identified in the membrane leakage experiments, as shown in Fig. 4*C*. This finding is consistent with the fact Gly-12 has been postulated to play an important structural role by adopting a positive φ-angle conformation favored in tight turns such as in loop 3 (41).

The trends noted in the location of residues that are important for lytic activity in phospholipid vesicles are very similar to those noted for hemolytic (18) and anthelmintic (15) activities. The combined findings thus suggest that a common mechanism is responsible for a range of cyclotide activities. Interestingly, the location of the residues forming the bioactive face does not correspond with a previously proposed membrane binding face for cyclotides.

NMR studies of cyclotide-membrane interactions led to the conclusion that a hydrophobic patch on the surface of kalata B1 formed by loop 5 (Trp-23, Pro-24, and Val-25) and loop 6 (Leu-2, Pro-3, and Val-4) assisted its binding to dodecylphosphocholine micelles (24). In this respect, single substitutions at these positions would be predicted to reduce the efficiency of membrane binding, a prediction that is confirmed by the vesicle leakage experiments reported herein (apart from for the Pro-24 mutant, which was insoluble and could not be examined).

This study is the first involving electrophysiological measurements of the interaction of kalata B1 and alanine mutants with asolectin liposomes and has enabled the demonstration of the channel-like activity of kalata B1 using the patch clamp technique. The current traces observed indicate that kalata B1 interacts with lipid membranes at concentrations down to 2.5 μM. Channel-like activity was observed for the majority of patches. The only dissimilarity in the leakage induced by different concentrations of kalata B1 was the onset time of channel opening, and hence leakage. The activity was observed to occur within 3 min when the micropipettes were backfilled with 25 μM kalata B1 solution, 5 min for 10 μM, and after 10 min for 2.5 μM. The time-dependent onset of channel-like activity suggests that kalata B1 progressively becomes sequestered on the membrane surface until a critical cyclotide concentration is reached, resulting in pore formation. The application of 25 μM kalata B1 caused consecutive, stepwise current increases. The four openings (O1, O2, O3, and O4) observed prior to the total disruption of the

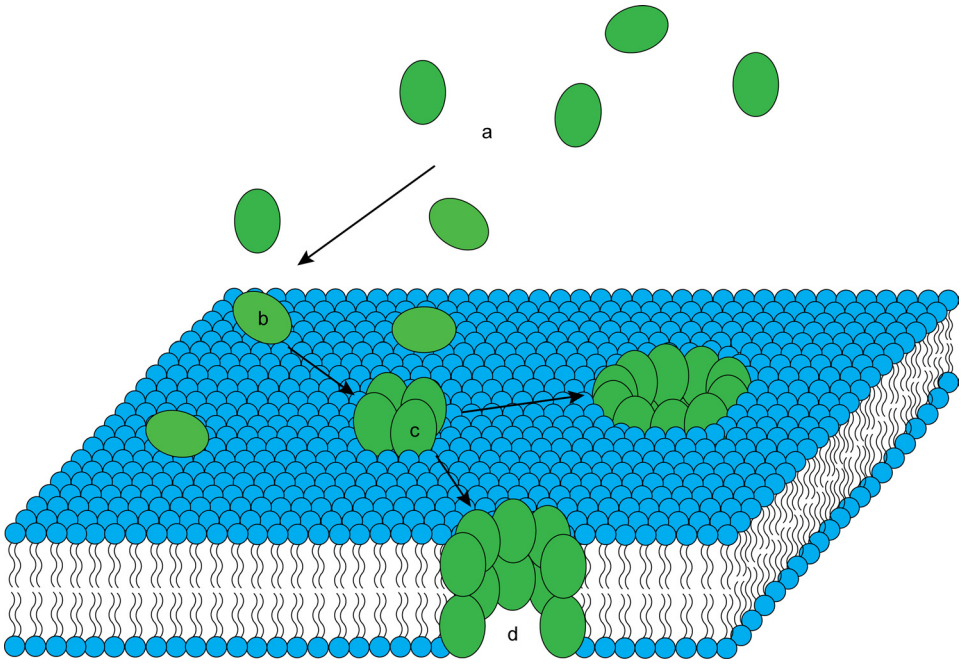

FIGURE 8. **Proposed model for pore formation in membranes by kalata B1.** Initial interactions occur between the hydrophobic patch of the kalata B1 and the membrane head groups. Kalata B1 then diffuses laterally to form oligomers (tetramers or octamers) followed by membrane-disruption involving pore-formation. *Arrows* in this figure show the transition from monomer in solution (*a*); to monomers in contact with the membrane surface (*b*); to tetramer formation (*c*); and final pore-formation (*d*).

liposome patch strongly support the suggestion that the lytic property of kalata B1 involves a pore-forming mechanism.

The measured fluctuations in currents in typical recordings suggest that cyclotide-induced formation of membrane pores is a dynamic process with progressive changes in the number of components forming the transmembrane structure (42). To estimate the diameter of the transmembrane pores formed by kalata B1 in the liposome patches, a conductance value was determined from the current-voltage plot. The determination of the size of a pore may give clues as to the mechanism of pore formation and the selectivity of an ion channel. The pore formed by kalata B1 was estimated to be 44 Å in diameter, fluctuating in the range 41–47 Å. This is much larger than typical ion channels, which explains the lack of selectivity observed (potassium, sodium, and *N*-methyl-D-glucamine ions) and the general leaky character of the pores.

The study of the kinetic interaction of kalata B1 with phospholipid vesicles demonstrated unequal association and dissociation rates of kalata B1. A reduction in the leakage of CF dye from loaded vesicles of ~50% was noted following a 30-min preincubation of kalata B1 with dye-free vesicles relative to experiments performed without preincubation. These results suggest that the association rate of kalata B1 with the lipid bilayer is higher than the dissociation rate, and that the peptide is sequestered on the membrane surface. Peptide sequestration is supported by the results described above in the patch clamp experiments in which the stepwise current increases are attributed to consecutive openings until total membrane disruption occurs.

Several alternative models for pore formation and membrane disruption have been proposed, mainly in the context of studies of antimicrobial peptides (42–44). In general, the mode of action of antimicrobial peptides involves initial electrostatic interactions of these usually cationic peptides with the negatively charged lipids. Hydrophobic interactions between non-polar amino acids and the hydrophobic core of the membrane then allow peptide insertion into the lipid bilayer. One model proposes that self-associating peptide monomers are involved in the formation of a transmembrane channel (Barrel-stave model) (45). Another model postulates the disintegration of the membrane via disruption of the bilayer curvature and the formation of torroidal pores (46). Kalata B1 contains only a single positively charged residue, and therefore its mode of action is unlikely to involve the formation of torroidal pores. In this study, the vesicle leakage experiments showed that (i) kalata B1 did not demonstrate preferential selection of anionic phospholipids over zwitterionic phospholipids in single lipid vesicles, and (ii) the peptide appears to be sequestered on the membrane surface prior to the initiation of membrane disruption. These results suggest that the most likely mode of action of kalata B1 is through a specific self-association model. It appears that this self-association is mediated by the "bioactive face" identified by the alanine mutagenesis experiments.

Fig. 8 represents our proposed pore formation model in which kalata B1 molecules initially interact with the membrane surface via their well defined hydrophobic patch. Kalata B1 molecules then diffuse laterally to form oligomers, with the oligomerization interface centered around the identified bioactive face, and this is followed by membrane-disruption involving pore-formation. The oligomers are most likely tetramers or octamers, which have been previously observed in analytical ultracentrifuge studies. The pore, estimated to be 44 Å in diameter, could result from oligomers composed of a ring of 4–6 tetramers. In support of this model, if lateral diffusion of the monomers is the rate-limiting step in oligomerization, and thus pore formation, the time needed for this to occur would decrease with increasing peptide concentration. Our data support this hypothesis, because the patch clamp experiments showed a decreased lag time with increased concentrations of kalata B1.

In summary, from this study it can be concluded that kalata B1 is a membrane-active and pore-forming peptide, characteristics that explain its lytic ability toward membrane mimetics and electrophysiological properties. An alanine scan showed several residues, particularly within loop 1, are critical for its lytic ability and are clustered on one face of the molecule. Kinetic analysis revealed that the kalata B1 is sequestered by the phospholipid vesicles and undergoes slow exchange between

vesicles. Patch clamp experiments demonstrated the concentration-dependent disruption of the membrane by both kalata B1 and select alanine mutants. No channel activity was observed for V25A-kB1, an inactive mutant, whereas channel activity similar to wild-type kalata B1 was noted for the active mutant T20A-kB1. The size of the pore formed for kalata B1 is 41–47 Å in diameter. Collectively, the findings of this study provide a mechanistic explanation for the diversity of biological functions ascribed to this fascinating family of peptidic molecules.

Acknowledgments—We thank Rekha Bharathi for extraction of cyclotides from plant material, Shane Simonsen for donation of some alanine mutants, and Sónia Henriques for constructive comments.

REFERENCES

1. Craik, D. J., Daly, N. L., Mulvenna, J., Plan, M. R., and Trabi, M. (2004) *Curr. Protein Pept. Sci.* **5,** 297–315
2. Craik, D. J. (2001) *Toxicon* **39,** 1809–1813
3. Colgrave, M. L., and Craik, D. J. (2004) *Biochemistry* **43,** 5965–5975
4. Craik, D. J., Daly, N. L., Bond, T., and Waine, C. (1999) *J. Mol. Biol.* **294,** 1327–1336
5. Gustafson, K. R., Sowder II, R. C., Henderson, L. E., Parsons, I. C., Kashman, Y., Cardellina II, J. H., McMahon, J. B., Buckheit, R. W., Jr., Pannell, L. K., and Boyd, M. R. (1994) *J. Am. Chem. Soc.* **116,** 9337–9338
6. Daly, N. L., Gustafson, K. R., and Craik, D. J. (2004) *FEBS Lett.* **574,** 69–72
7. Ireland, D. C., Wang, C. K., Wilson, J. A., Gustafson, K. R., and Craik, D. J. (2008) *Biopolymers* **90,** 51–60
8. Wang, C. K., Colgrave, M. L., Gustafson, K. R., Ireland, D. C., Goransson, U., and Craik, D. J. (2008) *J. Nat. Prod.* **71,** 47–52
9. Witherup, K. M., Bogusky, M. J., Anderson, P. S., Ramjit, H., Ransom, R. W., Wood, T., and Sardana, M. (1994) *J. Nat. Prod.* **57,** 1619–1625
10. Barry, D. G., Daly, N. L., Clark, R. J., Sando, L., and Craik, D. J. (2003) *Biochemistry* **42,** 6688–6695
11. Tam, J. P., Lu, Y. A., Yang, J. L., and Chiu, K. W. (1999) *Proc. Natl. Acad. Sci. U.S.A.* **96,** 8913–8918
12. Göransson, U., Sjögren, M., Svangård, E., Claeson, P., and Bohlin, L. (2004) *J. Nat. Prod.* **67,** 1287–1290
13. Jennings, C., West, J., Waine, C., Craik, D., and Anderson, M. (2001) *Proc. Natl. Acad. Sci. U.S.A.* **98,** 10614–10619
14. Jennings, C. V., Rosengren, K. J., Daly, N. L., Plan, M., Stevens, J., Scanlon, M. J., Waine, C., Norman, D. G., Anderson, M. A., and Craik, D. J. (2005) *Biochemistry* **44,** 851–860
15. Colgrave, M. L., Kotze, A. C., Huang, Y. H., O'Grady, J., Simonsen, S. M., and Craik, D. J. (2008) *Biochemistry* **47,** 5581–5589
16. Barbeta, B. L., Marshall, A. T., Gillon, A. D., Craik, D. J., and Anderson, M. A. (2008) *Proc. Natl. Acad. Sci. U.S.A.* **105,** 1221–1225
17. Colgrave, M. L., Kotze, A. C., Ireland, D. C., Wang, C. K., and Craik, D. J. (2008) *Chembiochem.* **9,** 1939–1945
18. Simonsen, S. M., Sando, L., Rosengren, K. J., Wang, C. K., Colgrave, M. L., Daly, N. L., and Craik, D. J. (2008) *J. Biol. Chem.* **283,** 9805–9813
19. Colgrave, M. L., Kotze, A. C., Kopp, S., McCarthy, J. S., Coleman, G. T., and Craik, D. J. (2009) *Acta Trop.* **109,** 163–166
20. Plan, M. R., Göransson, U., Clark, R. J., Daly, N. L., Colgrave, M. L., and Craik, D. J. (2007) *Chem. Bio. Chem.* **8,** 1001–1011
21. Nourse, A., Trabi, M., Daly, N. L., and Craik, D. J. (2004) *J. Biol. Chem.* **279,** 562–570
22. Kamimori, H., Hall, K., Craik, D. J., and Aguilar, M. I. (2005) *Anal. Biochem.* **337,** 149–153
23. Svangård, E., Burman, R., Gunasekera, S., Lövborg, H., Gullbo, J., and Göransson, U. (2007) *J. Nat. Prod.* **70,** 643–647
24. Shenkarev, Z. O., Nadezhdin, K. D., Sobol, V. A., Sobol, A. G., Skjeldal, L., and Arseniev, A. S. (2006) *FEBS J.* **273,** 2658–2672
25. Shenkarev, Z. O., Nadezhdin, K. D., Lyukmanova, E. N., Sobol, V. A., Skjeldal, L., and Arseniev, A. S. (2008) *J. Inorg. Biochem.* **102,** 1246–1256
26. Daly, N. L., and Craik, D. J. (2000) *J. Biol. Chem.* **275,** 19068–19075
27. Rex, S. (1996) *Biophys. Chem.* **58,** 75–85
28. Stewart, J. C. (1980) *Anal. Biochem.* **104,** 10–14
29. Yeaman, M. R., and Yount, N. Y. (2003) *Pharmacol. Rev.* **55,** 27–55
30. Schwarz, G., and Robert, C. H. (1990) *Biophys. J.* **58,** 577–583
31. Schwarz, G., and Robert, C. H. (1992) *Biophys. Chem.* **42,** 291–296
32. Häse, C. C., Le Dain, A. C., and Martinac, B. (1995) *J. Biol. Chem.* **270,** 18329–18334
33. Martinac, B., and Hamill, O. P. (2002) *Proc. Natl. Acad. Sci. U.S.A.* **99,** 4308–4312
34. de los Rios, V., Mancheño, J. M., Lanio, M. E., Oñaderra, M., and Gavilanes, J. G. (1998) *Eur. J. Biochem.* **252,** 284–289
35. Neher, E., and Sakmann, B. (1976) *Nature* **260,** 799–802
36. Neher, E., Sakmann, B., and Steinbach, J. H. (1978) *Pflugers Arch.* **375,** 219–228
37. Molleman, A. (2002) *Patch Clamping: an Introductory Guide to Patch Clamp Electrophysiology*, pp. 1–40, J. Wiley, New York
38. Hamill, O. P., Marty, A., Neher, E., Sakmann, B., and Sigworth, F. J. (1981) *Pflugers Arch.* **391,** 85–100
39. Aidley, D. J., and Stanfield, P. R. (1996) *Ion channels: Molecules in Action*, pp. 33–52, Cambridge University Press, Cambridge
40. Cruickshank, C. C., Minchin, R. F., Le Dain, A. C., and Martinac, B. (1997) *Biophys. J.* **73,** 1925–1931
41. Rosengren, K. J., Daly, N. L., Plan, M. R., Waine, C., and Craik, D. J. (2003) *J. Biol. Chem.* **278,** 8606–8616
42. Shai, Y. (1999) *Biochim. Biophys. Acta* **1462,** 55–70
43. Matsuzaki, K. (1999) *Biochim. Biophys. Acta* **1462,** 1–10
44. Zasloff, M. (2002) *Nature* **415,** 389–395
45. Ehrenstein, G., and Lecar, H. (1977) *Q. Rev. Biophys.* **10,** 1–34
46. Pouny, Y., Rapaport, D., Mor, A., Nicolas, P., and Shai, Y. (1992) *Biochemistry* **31,** 12416–12423
47. Craik, D. J., Daly, N. L., and Waine, C. (2001) *Toxicon* **39,** 43–60